Available online at www.sciencedirect.com
ScienceDirect
Trans. Nonferrous Met. Soc. China 31(2021) 913−924
Transactions of Nonferrous Metals Society of China
www.tnmsc.cn

Effect of NaOH concentration on microstructure and corrosion resistance of MAO coating on cast Al−Li alloy

Ying QIN[1], Guo-hua WU[1], Andrej ATRENS[2], Xiao-long ZHANG[1], Liang ZHANG[1], Wen-jiang DING[1]

1. National Engineering Research Center of Light Alloy Net Forming, State Key Laboratory of Metal Matrix Composites, School of Materials Science and Engineering, Shanghai Jiao Tong University, Shanghai 200240, China;
2. School of Mechanical and Mining Engineering, the University of Queensland, Brisbane Qld, 4072, Australia

Received 21 April 2020; accepted 8 January 2021

Abstract: Ceramic coating was prepared on cast Al−Cu−Li alloy by micro-arc oxidation (MAO) in a silicate electrolyte solution with additives including Na_2WO_4 and NaOH. The effect of NaOH addition varying from 1 to 9 g/L on the microstructure and corrosion behavior of the coatings was investigated. The coating was characterized by XRD, XPS and SEM with respect to the composition and microstructures. The results show that NaOH promoted the formation of oxides in the reaction of MAO and contributed to the increase of layer thickness. Electrochemical tests (polarization curve and EIS) and mass loss test indicate that the corrosion resistance of the coated Al−Cu−Li alloy was improved with the increased addition of NaOH. Moreover, the results prove that the alumina coating formed in the electrolyte with 7 g/L NaOH showed the best corrosion resistance. The examination of the full immersion corrosion test presents the same result of corrosion resistance.

Key words: Al−Cu−Li; NaOH; micro-arc oxidation; corrosion behavior

1 Introduction

Al−Li alloys are regarded as ideal structural materials for aircraft, aerospace, and national defense applications owing to their low density and high elastic modulus. For each 1 wt.% increment of Li addition to Al alloys (up to 4 wt.% Li addition), the density can be reduced by about 3% and the elastic modulus will be increased by about 6% simultaneously [1,2]. For example, pure aluminum has an elastic modulus of 70 GPa, while the elastic modulus of 2090 Al−Li alloy with 2.1 wt.% lithium is 79.7 GPa [3]. However, Al−Li alloy is prone to corrosion in wet and salt spray environments due to the activity of lithium [4−6]. Therefore, in order to prolong the service life, the surface protection treatment must be carried out for the alloys. Among the various means of surface treatment, micro-arc oxidation (MAO) may be one of the most efficient technologies. The ceramic coating composed of matrix metal oxide is deposited on the surface of the substrate alloy under the proper coordination of electrolyte and electrical parameters. Thanks to the existence of the ceramic phases and the interpenetration between the coating and the surface of the substrate, the obtained coating has excellent properties to prevent corrosion [7−9]. This promising technology has made it possible to overcome the shortcomings of Al, Mg, and Ti alloys in application fundamentally [10,11]. Previous studies suggested that the electrolyte has direct effects on the performance of the MAO coating [12]. The studies [13,14] on conventional aluminum alloys demonstrated that SiO_3^{2-} possesses good adsorption without pollution, WO_4^{2-} [15] serves the

Corresponding author: Guo-hua WU; Tel: +86-21-54742630; Fax: +86-21-34202794; E-mail: ghwu@sjtu.edu.cn
DOI: 10.1016/S1003-6326(21)65549-8

function of promoting the growth of film, and NaOH [16] is related to the conductivity of the solution and discharge process.

Little research has been focused on the MAO treatment of cast Al−Li alloys. The discharge process and the mechanism of MAO on 2A97 Al−Cu−Li alloy were studied by CHENG et al [17,18]. Available information [19] only provides the influence of electrical parameters on the thickness and corrosion resistance of the film. However, the electrolytes employed in the above studies were too simple to improve the corrosion resistance efficiently. As one of the most important process parameters of MAO, a suitable electrolyte can greatly improve the production efficiency and the corrosion resistance of the substrate. However, the electrolyte optimization for MAO of cast Al−Li alloys has not been researched in depth yet.

In this present study, Al−2Li−2Cu−0.2Zr alloy was selected as the base material because it exhibits good mechanical properties (yield strength of 142 MPa, ultimate tensile strength of 293 MPa, and elongation of 18.1%) according to our previous work [20]. Therefore, it is necessary to study the MAO process of this alloy to improve its corrosion resistance. Based on the previous studies of conventional aluminum alloys [12−16], Na_2SiO_3, Na_2WO_4 and NaOH were chosen as the main solutes of the electrolyte. Herein, the effect of NaOH concentration on the microstructure and corrosion resistance of Al−2Li−2Cu−0.2Zr alloy coated by MAO was analyzed. The corrosion behavior of MAO coating was studied systematically, and an MAO electrolyte suitable for improving the corrosion resistance of cast Al−Li alloy was successfully developed.

2 Experimental

2.1 Preparation of MAO coatings

The Al−2Li−2Cu−0.2Zr alloy (compositions in wt.%: 1.96 Li, 1.89 Cu, 0.1 Fe and balance Al) was selected as the substrate material with the dimension of 20 mm × 20 mm × 7 mm. Prior to the MAO treatment, the specimens were ground to 180#, 1200# and 2000# grit SiC paper in turn, and dried after rinsing with alcohol and deionized water. The electrolyte was prepared from distilled water containing 12 g/L Na_2SiO_3, 4 g/L Na_2WO_4, and some amount of NaOH. The composition of the electrolyte prepared with different concentrations of NaOH is given in Table 1.

Table 1 Electrolyte composition of MAO of Al−Li alloys

Sample No.	$w(Na_2SiO_3)$/ ($g\cdot L^{-1}$)	$w(Na_2WO_4)$/ ($g\cdot L^{-1}$)	w(NaOH)/ ($g\cdot L^{-1}$)
1	12	4	1
2	12	4	3
3	12	4	5
4	12	4	7
5	12	4	9

The oxidation treatment was conducted on MAO−60A equipment below 40 °C. The specimens of Al−2Li−2Cu−0.2Zr alloy were used as the anode while the wall of the stainless-steel container served as the cathode. According to long-term practical experience, the positive and negative duty cycles were 20% and 50%, respectively, and the pulse frequency was set at 2000 Hz. A constant current density of 6 A/dm^2 was maintained for 10 min by controlling a bipolar pulse power supply.

2.2 Characterization

The phase compositions of the MAO coating were characterized by X-ray diffraction (XRD, Rigaku Ultima IV) on the specimen surface scanning in the range of 2θ=10°–90° with an angular velocity of 4 (°)/min. The compositions of the near-surface region of the coatings were also analyzed by X-ray photoelectron spectroscopy (XPS), using monochromatic Al target, Al K_α ray, with binding energy calibrated according to C 1s peak. All of the surface and cross-section morphologies of the coatings were observed by scanning electron microscopy (SEM, Phenom XL) in secondary electron mode. The micro-area composition was analyzed by an energy dispersive spectrometer (EDS). Potentiodynamic polarization and electrochemical impedance spectroscopy (EIS) techniques were employed to study the corrosion behavior of the coatings by PARSTAT 2273 electrochemical workstation in 3.5 wt.% NaCl solution. The open circuit potential was measured immediately after soaking for 1 h, followed by a record of the polarization curve. The working electrode was the coated sample with an area of 4 cm^2, with the graphite electrode and saturated calomel electrode (SCE) served as the auxiliary

electrode and reference electrode, respectively. Four same samples were selected for a synchronous experiment in 3.5 wt.% NaCl solution, with three for mass loss measurement and one for observation of corrosion morphology, which lasted for 600 h. The mass of the samples was recorded after cleaning every 48 h. The effect of NaOH concentration in the electrolyte on the coating and the optimization of the formula would be determined by the aforementioned characterization methods.

3 Results and discussion

3.1 Phase composition

Figure 1 illustrates that the major phases of the MAO coating were the unstable γ-Al_2O_3 and stable α-Al_2O_3 phase at high temperature. The strong diffraction peaks of Al were attributed to the defects of the coating. In addition, there was a diffraction peak of θ-Al_2O_3 phase with low intensity which is a transition phase from γ-Al_2O_3 to α-Al_2O_3 [21].

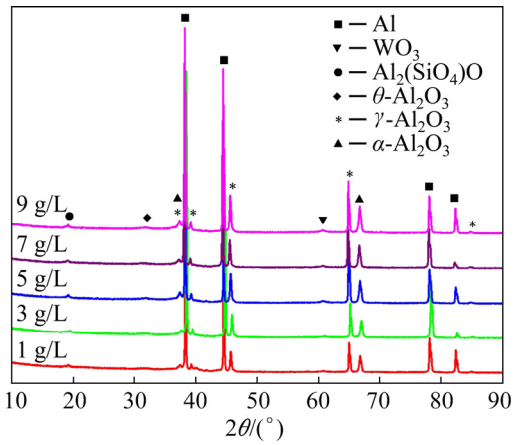

Fig. 1 X-ray diffraction patterns of coatings prepared in electrolytes with different concentrations of NaOH

$Al_2(SiO_4)O$, a phase commonly known as andalusite [22] also existed, which was formed by silicate ions in the electrolyte and aluminum matrix with the action of the high temperature of MAO. WO_3 phase could be generated by the following reactions [23] between sodium tungstate and aluminum, accompanied by the oxidation of aluminum alloy to form a film at the same time:

$$2WO_4^{2-}-4e \rightarrow 2WO_3+O_2\uparrow \quad (1)$$

$$WO_3+2Al \rightarrow Al_2O_3+W \quad (2)$$

The XRD results indicate that NaOH was not reflected directly in the phase composition, but influenced the reaction process remarkably. With the increase of NaOH concentration, more microscopic channels opened with more solutes involved in the reaction, which facilitated the growth of the oxidation. Therefore, the intensity of the diffraction peaks of γ-Al_2O_3 and $Al_2(SiO_4)O$ became stronger.

XPS was applied to determining whether lithium existed in the film. After ten tests, the selected map of the Li region is shown in Fig. 2, with no obvious Li 1s signal detected. This means that Li was not involved in the reaction of MAO.

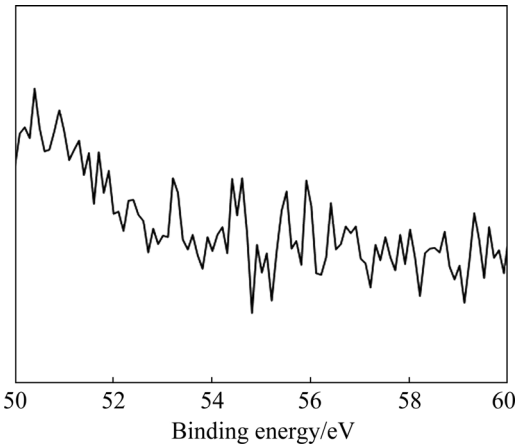

Fig. 2 Li 1s scanning map of MAO film by XPS

3.2 Microstructure

The morphologies of the surface and corresponding cross-section of Al−Li alloys coated are presented in Fig. 3 and Fig. 4, respectively. A large number of round pores distributed all over the surface, which was similar to the morphology of volcanic eruption. The fine particles dispersed on the surface and adhered to each other, especially in Fig. 3(a). Such particles spread on the relatively flat surface, accompanied by hairline cracks. The number of holes per unit area decreased and the micro-cracks faded away with increasing the NaOH concentration, as confirmed by Figs. 3(b, c, d). The irregular voids and the appearance of deep cracks appeared in Sample 5 (Fig. 3(e)), which was characterized by the flaky ablation marks and partial shedding pointed out by Mark A.

Through the observation of the cross-sectional morphologies, it is apparent that the concentration of NaOH in electrolyte had a great influence on the thickness of the coating. The increase of NaOH concentration sped up the growth of the film and

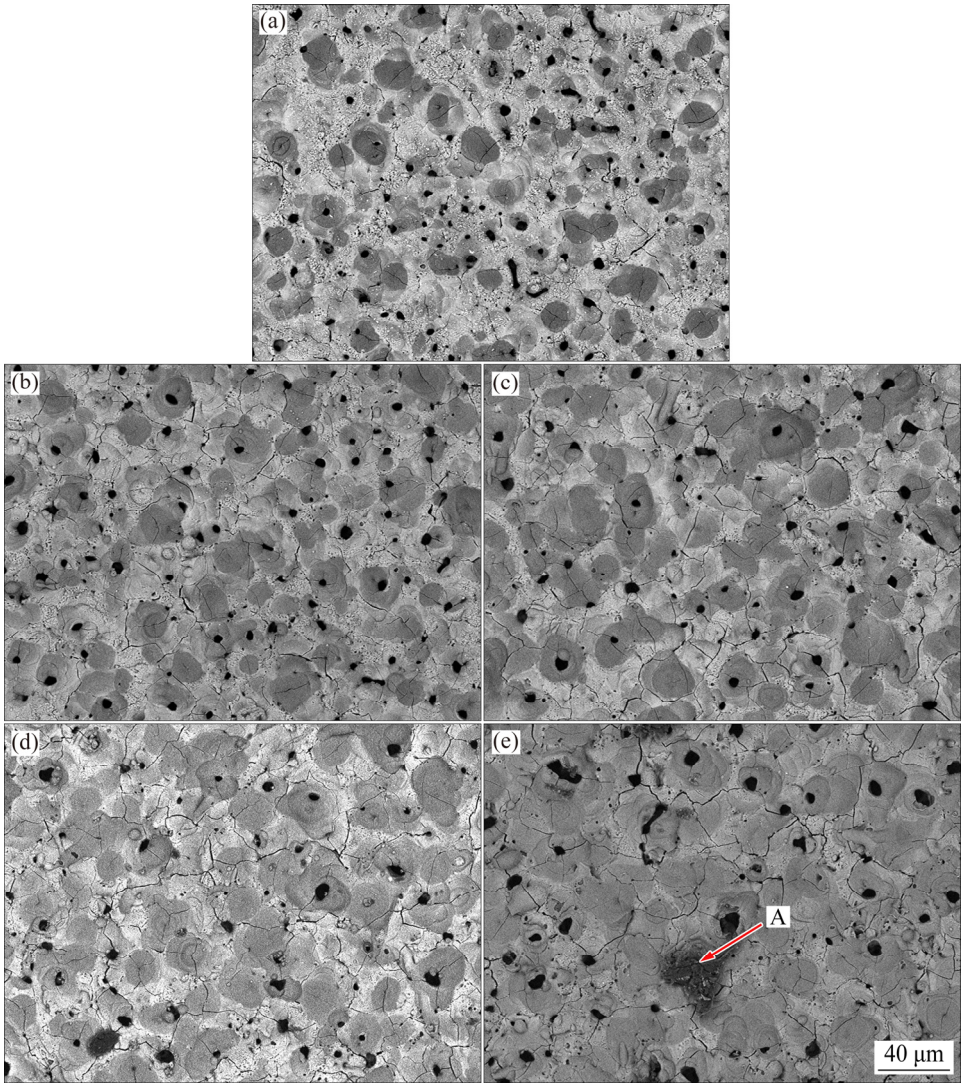

Fig. 3 Surface morphologies of samples prepared in electrolytes with different concentrations of NaOH: (a) 1 g/L; (b) 3 g/L; (c) 5 g/L; (d) 7 g/L; (e) 9 g/L (A−Flaky ablation)

reduced the proportion of voids in the coating. Figure 4(d) illustrates that the relatively dense coating was obtained by using the MAO electrolyte containing 7 g/L NaOH. The circular or flat holes did not connect mutually, indicating that the coating grew continuously and was closely integrated with each other. Mark B in Fig. 4(e) shows the broken part of the film and a rupture between the surface and the dense layer.

According to the XPS results, lithium did not participate in the reaction during MAO process. However, considering the poor stability of lithium in an aqueous solution at high temperature, the precipitation of lithium resulted in a large number of defects in the anode film at the beginning [24,25]. On the other hand, the bubble expanded with the growth of the coating and gas was released when the rupture occurred. Then, the increase of thickness and occurrence of dielectric breakdown followed. These two effects provoked the enhancement of the electric field and strong micro-discharge, which possessed an immediate impact on the defects on the cross-section [26,27].

The NaOH played a critical role in the process of MAO by increasing the electrical conductivity of the bath solution and accelerating the spark discharge over the alloy surface [28]. The instantaneous temperature in the spark region might come up to 10^3−10^4 °C [6], which allows the ions of the electrolyte in the free passage of the discharge channel. The increase of sodium hydroxide brought about more swimming ions, and the strong alkalinity of the solution was beneficial to the breakdown. At the initial stage of MAO, the voltage

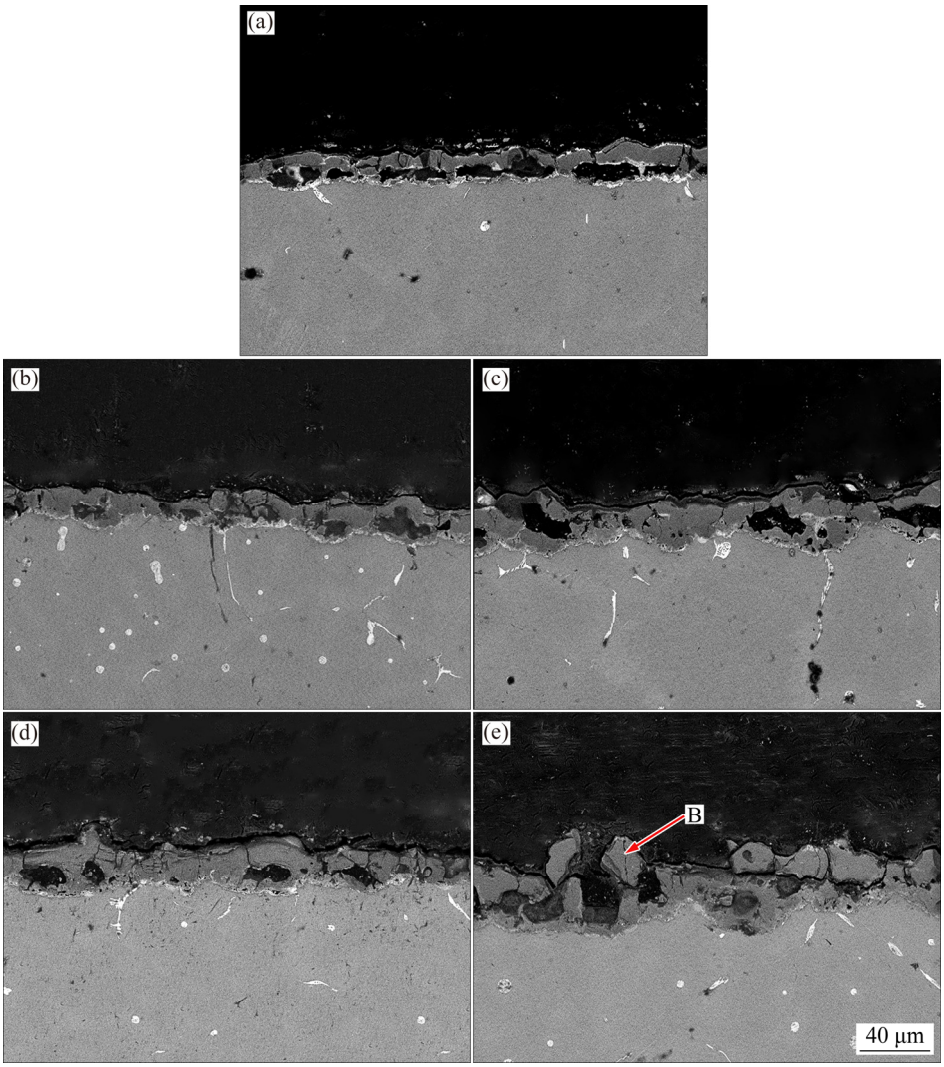

Fig. 4 Cross-sectional morphologies of samples prepared in electrolytes with differetn concentrations of NaOH: (a) 1 g/L; (b) 3 g/L; (c) 5 g/L; (d) 7 g/L; (e) 9 g/L (B−Broken part from layer)

rose sharply. Sparks appeared on the surface once it reached the arc-starting voltage, and then the voltage continued to rise modestly and finally stabilized at a fixed value. As shown in Fig. 5 and Table 2, with the increase of NaOH concentration, the arc striking voltage was reduced and the effective voltage of micro-arc discharge was increased, which expedited the film formation of the layer.

Nevertheless, excessive NaOH generated an unstable or inconsecutive reaction and resulted in the formation of microscopic ablation spots. Point discharge produced by non-uniform spark could generate localized disruption to the ceramic film as exemplified by Fig. 4(e). On the other hand, even though NaOH was beneficial to the growth of coating, the increase of pH value would lead to the dissolution of the layer. The disconnection between loose layers emerged obviously and the compact layer could hardly become thicker.

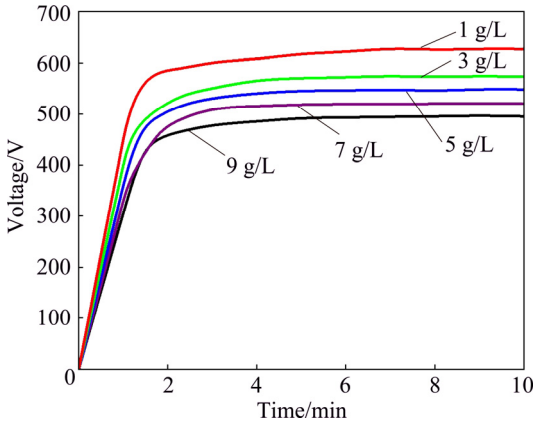

Fig. 5 Voltage−time curves of MAO with different NaOH concentrations

Table 2 Striking and final voltages of MAO with different NaOH concentrations

ρ(NaOH)/(g·L^{-1})	Striking voltage/V	Final voltage/V
1	453	626
3	402	573
5	361	548
7	329	522
9	313	496

3.3 Electrochemical behavior

3.3.1 Polarization curves

Figure 6 and Table 3 present the polarization curves of the Al−Li alloy and the samples prepared in the electrolyte with different concentrations of NaOH. The key factor affecting the corrosion resistance was the defects on the section instead of the holes on the surface. The corrosion potential only fluctuated slightly, while the corrosion current density that directly characterizes the corrosion rate differed distinctly. By comparison, the corrosion resistance of Sample 4 was the highest with the corrosion current density of 0.066 μA/cm^2, which was also consistent with the microstructure shown in Figs. 3 and 4.

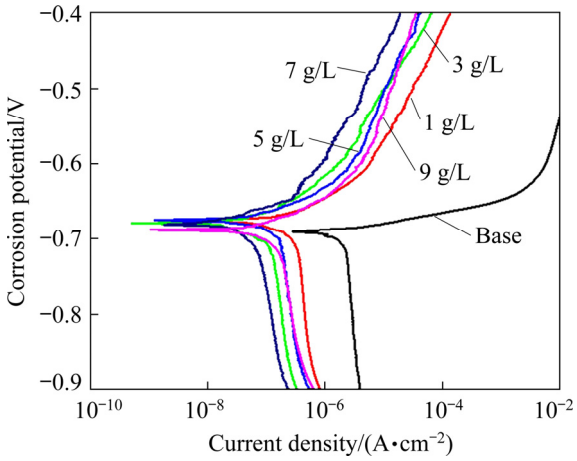

Fig. 6 Polarization curves of Al−Li alloys uncoated (base) and coatings prepared in electrolyte with different concentrations of NaOH

Table 3 Dynamic polarization parameters of Al−Li alloy and coatings prepared in electrolytes with different concentrations of NaOH

Sample	φ_{corr}/mV	J_{corr}/(μA·cm^{-2})
1	−675	0.289
2	−679	0.102
3	−676	0.154
4	−680	0.066
5	−689	0.093
Base	−692	2.072

3.3.2 EIS after long-time immersion

Considering the non-uniformity of the coating, the impedance value measured under the condition of open-circuit potential was unable to reflect the real situation of the film accurately. Therefore, the method of long-time immersion was used to measure the impedance value regularly in 280 h in order to characterize the corrosion evolution. Figure 7 illustrates the electrochemical impedance spectra of the MAO specimens soaked in 3.5 wt.% NaCl solution for 1, 5, 10, 24, 48, 120 and 280 h. The Nyquist diagram containing two capacitive arcs represents that the time constants at high and low frequency corresponding to the outer layer and inner layer of MAO ceramic coating, respectively. The increase of charge transfer resistance in the corrosion process matched with extended capacitive arc radius in Nyquist diagram [29,30].

Figure 7 indicates that the corrosion process could be divided into two stages and fitted by two equivalent circuits. Considering the dispersion effect caused by the inhomogeneity of the electrode surface and the poor conductivity of the solution, the constant phase angle element Q was employed instead of C for fitting in these circuits [31]. The first stage of corrosion behavior, except for Sample 1, was explained by Fig. 8(a). The solution resistance was denoted by R. R_p and Q_p corresponded to the outer resistance and capacitance of the MAO ceramic layer, and those of the inner layer were represented by Q_d and R_d respectively. Within immersion time of 48 h, all of them were in the first stage of corrosion. However, both Samples 2 and 3 entered the second stage characterized by the typical Warburg diffusion in the low-frequency region of Nyquist diagram after 120 h. On account of the fact that the interface of the oxide film was corroded gradually with the extension of time, corrosion products accumulated and restricted the penetration of the medium, which led to Warburg diffusion. The higher the admittance coefficient W (Warburg), Y_0, the faster the diffusion process. Therefore, the corrosion process at this stage could be fitted by the model in Fig. 8(b). After immersion for 280 h, all of the samples entered the second stage of corrosion with Warburg diffusion. The specific parameters are listed in Table 4.

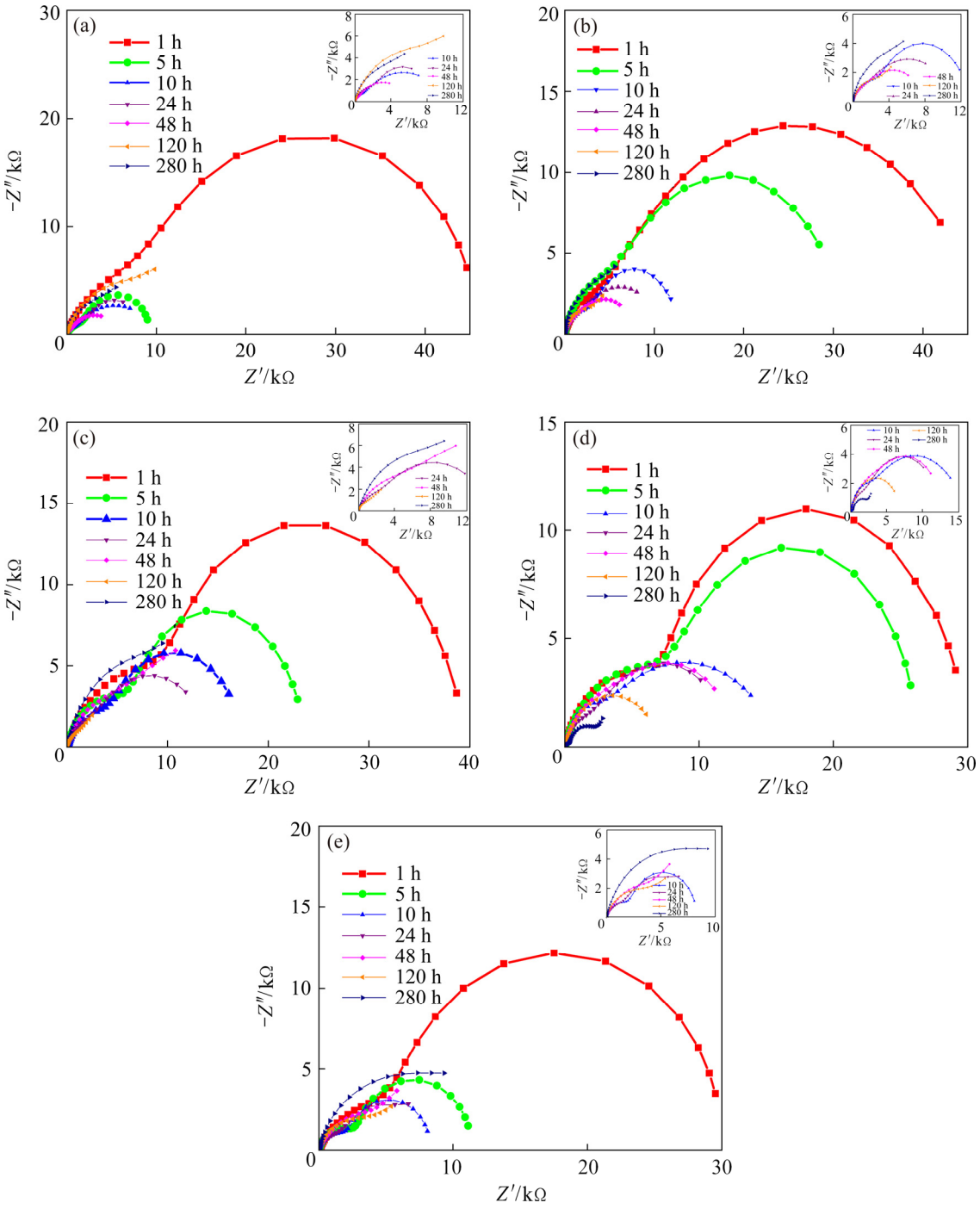

Fig. 7 EIS plots of coating prepared in electrolytes with different concentrations of NaOH immersed in 3.5% NaCl solution: (a) 1 g/L; (b) 3 g/L; (c) 5 g/L; (d) 7 g/L; (e) 9 g/L

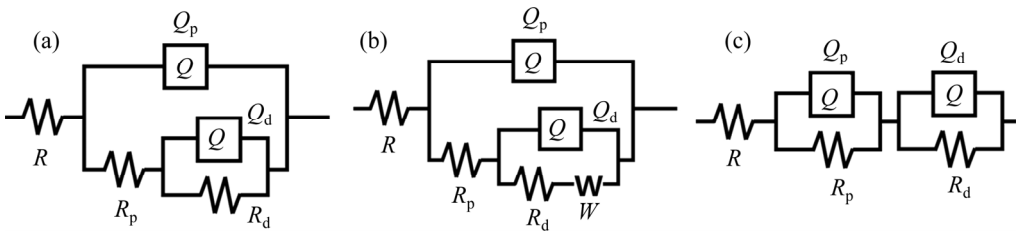

Fig. 8 Equivalent circuits of coated Al−Li alloy immersed in 3.5% NaCl solution: (a) First stage; (b) Second stage; (c) Series model

However, the disparity between the equivalent circuit in Fig. 8(a) and Nyquist plot of Sample 1 cannot be neglected, which was related to the structure of the layer. An obvious flat hole was observed at the interface between the substrate and the film layer in Fig. 4(a), which separated the substrate alloy and the film, so a series model exhibited in Fig. 8(c) was more precise. After 120 h of soaking, the gap between the loose layer and internal film was destroyed by corrosion products, and the model in Fig. 8(b) was still proper here. The changes of each parameter of Sample 1 are illustrated in Table 5.

With the further corrosion of the second stage, the corrosion products deposited between the solution and the dense layer. After the corrosion products accumulated to a certain amount, then they were dissolved. Meantime, the value of R_d rose at the beginning and then declined. The resistance of R_p was equivalent to a single digit, indicating that

Table 4 Electrochemical impedance spectroscopy parameters of MAO coatings prepared in electrolyte with different concentrations of NaOH

Sample No.	Immersion time/h	Q_p/ ($F\cdot cm^{-2}$)	n_1	R_p/ ($\Omega\cdot cm^2$)	Q_d/ ($F\cdot cm^{-2}$)	n_2	R_d/ ($\Omega\cdot cm^2$)	Y_0/ ($S\cdot s^{0.5}\cdot cm^{-2}$)
2	1	6.59×10^{-6}	0.714	6.27×10^{3}	2.99×10^{-5}	0.668	4.13×10^{4}	−
2	5	2.00×10^{-5}	0.779	9.09×10^{3}	8.19×10^{-5}	0.899	2.31×10^{4}	−
2	10	3.33×10^{-5}	0.791	3.61×10^{3}	2.35×10^{-4}	0.830	9.43×10^{3}	−
2	24	8.65×10^{-5}	0.780	2.21×10^{3}	3.21×10^{-4}	0.629	9.14×10^{3}	−
2	48	9.253×10^{-3}	0.56	0.783	2.58×10^{-3}	0.516	0.677	−
2	120	8.38×10^{-5}	0.917	10.78	2.31×10^{-4}	0.777	2.96×10^{3}	1.37×10^{-3}
2	280	2.18×10^{-4}	0.882	7.58	3.39×10^{-4}	0.88	5.33×10^{3}	9.47×10^{-4}
3	1	9.36×10^{-6}	0.719	1.44×10^{4}	4.14×10^{-5}	1	2.55×10^{4}	−
3	5	1.95×10^{-5}	0.774	8.53×10^{3}	1.32×10^{-4}	1	1.53×10^{4}	−
3	10	4.10×10^{-5}	0.748	6.16×10^{3}	2.34×10^{-4}	0.926	1.16×10^{4}	−
3	24	8.05×10^{-5}	0.748	4.51×10^{3}	2.9×10^{-4}	0.803	1.00×10^{4}	−
3	48	1.29×10^{-4}	0.756	7.26×10^{3}	5.32×10^{-4}	0.618	2.36×10^{4}	−
3	120	1.55×10^{-4}	0.876	8.31	1.62×10^{-4}	0.834	8.4×10^{3}	4.67×10^{-4}
3	280	1.03×10^{-4}	0.842	79.75	9.20×10^{-5}	0.922	7.88×10^{3}	4.46×10^{-4}
4	1	9.64×10^{-6}	0.778	9.38×10^{3}	6.66×10^{-5}	1	2.07×10^{4}	−
4	5	1.62×10^{-5}	0.750	1.04×10^{4}	1.18×10^{-4}	0.988	1.66×10^{4}	−
4	10	3.20×10^{-5}	0.750	7×10^{3}	2.51×10^{-4}	1	7.01×10^{3}	−
4	24	7.31×10^{-5}	0.831	3.03×10^{3}	3.4×10^{-4}	0.764	9.7×10^{3}	−
4	48	1.01×10^{-4}	0.766	6.78×10^{3}	4.58×10^{-4}	0.836	6.25×10^{3}	−
4	120	3×10^{-4}	0.727	0.967	2.82×10^{-5}	1	7.09×10^{3}	−
4	280	1.33×10^{-4}	0.553	402.8	3.26×10^{-4}	0.871	2.16×10^{3}	3.11×10^{-3}
5	1	2.19×10^{-5}	0.722	6.62×10^{3}	10^{-4}	1	1.32×10^{4}	−
5	5	3.57×10^{-5}	0.779	3.95×10^{3}	2.69×10^{-4}	0.988	7.12×10^{3}	−
5	10	5.88×10^{-5}	0.783	2.59×10^{3}	3.8×10^{-4}	0.886	6.38×10^{3}	−
5	24	1.23×10^{-4}	0.761	2.16×10^{3}	4.64×10^{-4}	0.696	8.75×10^{3}	−
5	48	1.22×10^{-4}	0.761	2.12×10^{3}	4.53×10^{-4}	0.711	6.67×10^{3}	−
5	120	2.61×10^{-4}	0.794	5.1×10^{3}	4.71×10^{-3}	1	6.05×10^{3}	−
5	280	1.27×10^{-4}	0.852	13.97	1.79×10^{-4}	0.844	10^{4}	1.88×10^{-3}

Table 5 Electrochemical impedance spectroscopy parameters of MAO coatings prepared in electrolyte with 1 g/L NaOH

Immersion time/h	Q_d/ ($F\cdot cm^{-2}$)	n_1	R_d/ ($\Omega\cdot cm^2$)	Q_p/ ($F\cdot cm^{-2}$)	n_2	R_p/ ($\Omega\cdot cm^2$)	Y_0/ ($S\cdot s^{0.5}\cdot cm^{-2}$)
1	8.02×10^{-5}	1	3.44×10^{4}	2.35×10^{-5}	0.735	1.14×10^{4}	–
5	9.39×10^{-5}	0.683	2.39×10^{3}	4.44×10^{-4}	1	6.88×10^{3}	–
10	9.28×10^{-5}	0.916	643.8	3.61×10^{-4}	0.649	9.44×10^{3}	–
24	2.24×10^{-4}	0.851	430.5	4.49×10^{-4}	0.811	5.72×10^{3}	–
48	1.92×10^{-4}	1	192.9	8.11×10^{-4}	0.69	5.79×10^{3}	–
120	3.42×10^{-4}	0.93	210.7	5.06×10^{-4}	0.743	1.5×10^{3}	1.5×10^{-3}
280	2.22×10^{-4}	1	16.69	3.78×10^{-4}	0.825	5.36×10^{3}	8.6×10^{-4}

the loose layer lost the protective effect at this moment. NaOH was negative to the density and smoothness of the surface layer, so the resistance decreased with the increase of concentration at the initial stage. However, the continuous growth of the film was facilitated effectively, which prolonged the time to reach the second stage of corrosion. Hence, the impedance tended to decrease steadily rather than sharply during the whole process.

3.4 Mass loss

The surface of the specimens was covered with fine bubbles at the beginning of the test, and then the flocculent white precipitation turned up and suspended in the solution. According to the trend of curves in Fig. 9, the process of the mass loss altered in line with the microstructure. For the first few days, it was apparent that the sample incurred a mass loss because of the unstable structure of the loose part. After that, a platform period was encountered, exhibiting the deceleration of mass loss. Over a period of days, the deposition of corrosion production was dissolved, which was manifested as the increase of mass loss. The mass loss of Sample 4 deposited in the solution with 7 g/L NaOH was the least with the relatively steady curve by comparison.

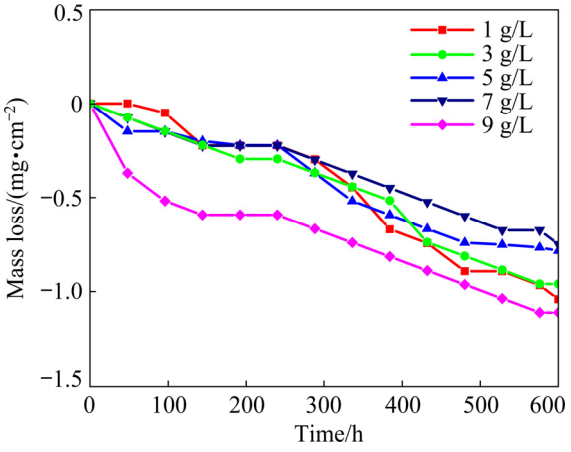

Fig. 9 Mass loss curves of coating prepared in electrolytes with different concentrations of NaOH

3.5 Full immersion corrosion test

Figure 10 provides the microstructures after the full immersion corrosion test in 3.5% NaCl solution for 600 h. The linear corrosion pits occupied the surface of Sample 1, connecting the crater holes and corrosion products gathering together. In the samples prepared in the solution with a higher concentration of NaOH, the accumulation of corrosion reduced significantly, but the cracks (Mark B) visibly propagated. Especially in Fig. 10(c), the undulating layer caused the thin part of the film more likely to be damaged and split in the process of soaking, which explained why the corrosion resistance of Sample 3 is inferior. Consistent with the description in corrosion tests, the coating was corroded mildly, as displayed in Fig. 10(d), which prevented the infiltration of the etching solution effectively. For the thickness of the layer of Sample 5, the corrosion target was more at the surface, resulting in the dissolution of a uniform bulk of the layer.

The EDS analysis of Point A at the corrosion morphology in Table 6 indicates that there was residue chlorine on the surface. For the long-time immersion test, Cl^- permeated into the micropores through competitive adsorption to promote the dissolution of the γ-Al_2O_3. Due to the existence of a small number of penetrating pores, part of Al−Li alloys contacted with the external medium directly and reacted with NaCl solution, which was responsible for pitting corrosion in the alloy directly.

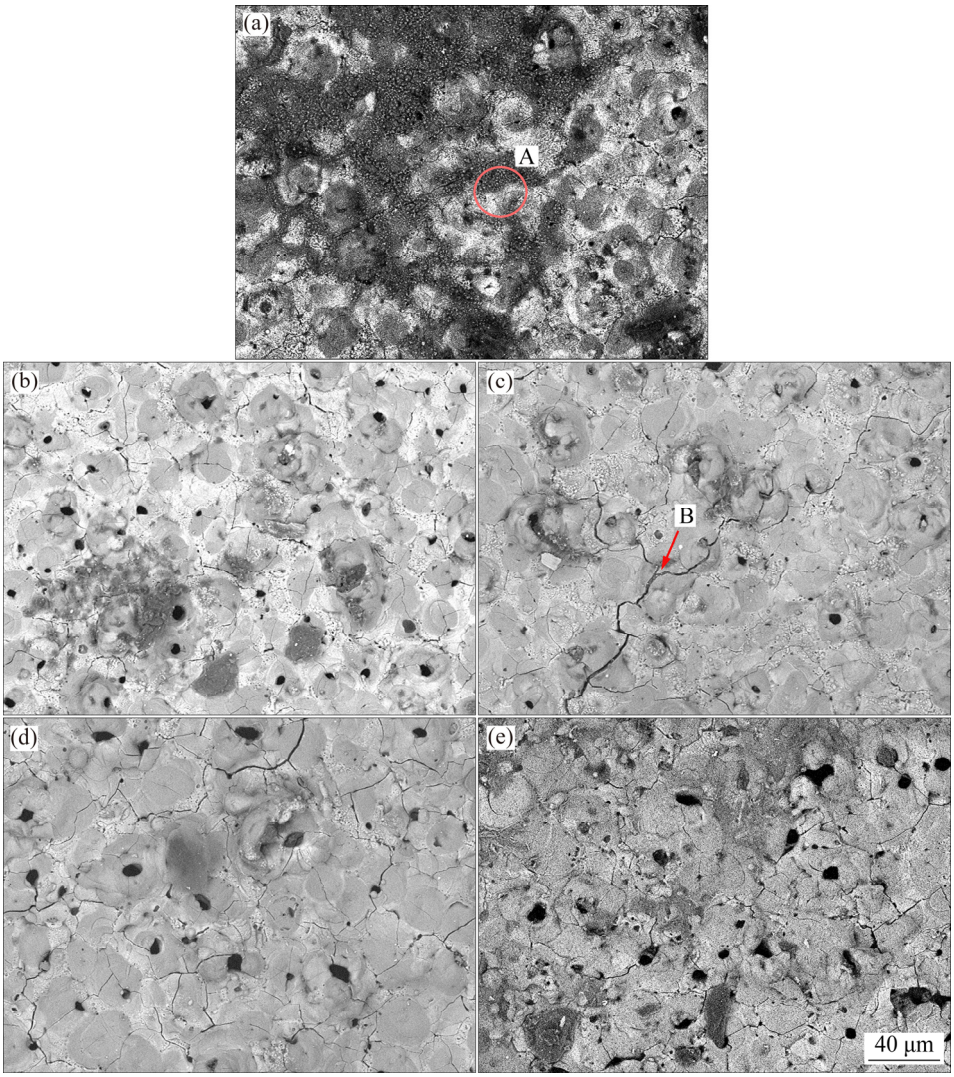

Fig. 10 SEM images of coating prepared in electrolytes with varied concentrations of NaOH after corrosion: (a) 1 g/L; (b) 3 g/L; (c) 5 g/L; (d) 7 g/L; (e) 9 g/L

Table 6 EDS elemental analysis of Point A

Element	Content/wt.%
O	83.47
Al	21.81
Cl	3.93

The resulting $AlCl_3$ went into the solution in the opposite direction. Both two reasons made for the existence of Cl.

4 Conclusions

(1) The increase of NaOH concentration in the electrolyte had a positive effect on the formation of γ-Al_2O_3 and $Al_2(SiO_4)O$ in the MAO coating on Al−Cu−Li alloy, without new phase produced.

(2) NaOH was beneficial to the increase of the thickness and continuous growth of the coating. However, NaOH also tended to cause the looseness of the outer layer because of the intense discharge.

(3) The corrosion process of MAO film was divided into two stages, comprised of the failure of the loose layer and the accumulation of corrosion products. With the increase of NaOH concentration, the time to enter the second stage of corrosion was delayed.

(4) When the electrolyte was composed of 12 g/L Na_2SiO_3, 4 g/L Na_2WO_4, and NaOH, the corrosion resistance of the coating samples was improved with the concentration of NaOH and the highest was achieved at 7 g/L. The corrosion current density was 0.066 μA/cm^2, which was much superior to the base alloy (J_{corr}=2.072 μA/cm^2).

Acknowledgments

This work is supported by the National Natural Science Foundation of China (51871148, 51821001), the United Fund of National Department of Education and Equipment Development (6141A02033245), and the National Key R&D Program of China (2016YFB0301003).

References

[1] DUAN Hong-ping, DU Ke-qin, YAN Chuan-wei, WANG Fu-hui. Electrochemical corrosion behavior of composite coatings of sealed MAO film on magnesium alloy AZ91D [J]. Electrochimica Acta, 2006, 51(14): 2898−2908.

[2] RIOJA R J, LIU J. The evolution of Al−Li base products for aerospace and space applications [J]. Metallurgical & Materials Transactions A, 2012, 43(9): 3325−3337.

[3] ELAGIN V I, ZAKHAROV V V. Modern Al−Li alloys and prospects of their development [J]. Metal Science and Heat Treatment, 2013, 55(3): 184−190.

[4] GAO Yong, ZHOU Yong-jin, ZHANG Rui-bin, CHEN Yan-yong. Discussion on anti-corrosion of torpedo wet-storage [J]. Ship Science & Technology, 2011, 33(6): 86−89.

[5] LI Jin-feng, ZHENG Zi-qiao, REN Wen-da, CHEN Wen-jing, ZHAO Xu-shan, LI Shi-chen. Simulation on function mechanism of *T*1(Al_2CuLi) precipitate in localized corrosion of Al−Cu−Li alloys [J]. Transactions of Nonferrous Metals Society of China, 2006, 16(6): 1268−1273.

[6] MORAN J P, BOVARD F S, CHRZAN J D, VANDENBURGH P. Corrosion performance of new generation aluminum−lithium alloys for aerospace applications [C]//WEILAND H, ROLLETT A D, CASSADA W A. ICAA13. Pittsburgh, PA: TMS, 2016: 425−430.

[7] YEROKHIN A L, NIE X, LEYLAND A, MATTHEWS A, DOWEY S J. Plasma electrolysis for surface engineering [J]. Surface and Coatings Technology, 1999, 122(2): 73−93.

[8] XIE Huan-jun, CHENG Ying-liang, LI Shao-xian, CAO Jin-hui, CAO Li. Wear and corrosion resistant coatings on surface of cast A356 aluminum alloy by plasma electrolytic oxidation in moderately concentrated aluminate electrolytes [J]. Transactions of Nonferrous Metals Society of China, 2017, 27(2): 336−351.

[9] YEROKHIN A, SNIZHKO L, GUREVINA N, LEYLAND A, PILKINGTON A, MATTHEWS A. Discharge characterization in plasma electrolytic oxidation of aluminium [J]. Journal of Physics D: Applied Physics, 2003, 36(17): 2110−2120.

[10] LUGOVSKOY A, ZINIGRAD M, KOSSENKO A, KAZANSKI B. Production of ceramic layers on aluminum alloys by plasma electrolytic oxidation in alkaline silicate electrolytes [J]. Applied Surface Science, 2013, 264: 743−747.

[11] KHANMOHAMMADI H, ALLAHKARAM S, TOWHIDI N. Microstructural, corrosion and mechanical behavior of two-step plasma electrolyte oxidation ceramic coatings [J]. Transactions of Nonferrous Metals Society of China, 2017, 27(10): 2225−2233.

[12] LIU Wan-ying, LIU Ying, LIN Yuan-hua, ZHANG Zhi, FENG Shao-bo, TALHA M, SHI Yun-sheng, SHI Tai-he. Effects of graphene on structure and corrosion resistance of plasma electrolytic oxidation coatings formed on D16T Al alloy [J]. Applied Surface Science, 2019, 475: 645−659.

[13] BECERIK D A, AYDAY A, KUMROUGLU L C, KURNAZ S C, OZEL A. The Effects of Na_2SiO_3 concentration on the properties of plasma electrolytic oxidation coatings on 6060 aluminum alloy [J]. Journal of Materials Engineering & Performance, 2012, 21(7): 1426−1430.

[14] CAO Fa-he, LIN Long-yong, ZHANG Zhao, ZHANG Jian-qing, CAO Chu-nan. Environmental friendly plasma electrolytic oxidation of AM60 magnesium alloy and its corrosion resistance [J]. Transactions of Nonferrous Metals Society of China, 2008, 18(2): 240−247.

[15] STOJADINOVIC S, VASILIC R, BELCA I, PETKOVIC M, KASALICA B, NEDIC Z, ZEKOVIC L. Characterization of the plasma electrolytic oxidation of aluminium in sodium tungstate [J]. Corrosion Science, 2010, 52(10): 3258−3265.

[16] DOOLABI D S, EHTESHAMZADEH M, MIRHOSSEINI S M M. Effect of NaOH on the structure and corrosion performance of alumina and silica PEO coatings on aluminum [J]. Journal of Materials Engineering & Performance, 2012, 21(10): 2195−2202.

[17] CHENG Ying-liang, MAO Mo-ke, CAO Jin-hui, PENG Zhao-mei. Plasma electrolytic oxidation of an Al−Cu−Li alloy in alkaline aluminate electrolytes: A competition between growth and dissolution for the initial ultra-thin films [J]. Electrochimica Acta, 2014, 138: 417−429.

[18] CHENG Ying-liang, CAO Jin-hui, MAO Mo-ke, XIE Huan-jun, SKELDON P. Key factors determining the development of two morphologies of plasma electrolytic coatings on an Al−Cu−Li alloy in aluminate electrolytes [J]. Surface and Coatings Technology, 2016, 291: 239−249.

[19] ZHAO Zhi-long, LIU Yi-yang, YAN Guang-ming. Research on properties of ceramic coating on 2090 Al−Li alloy by micro-arc oxidation [J]. Electroplating & Pollution Control, 2008, 27(5): 36−38.

[20] RONG Mian, ZHANG Liang, WU Guo-hua, LI Wei-wei, ZHANG Xiao-long, SUN Jiang-wei, DING Wen-jiang. Effect of refining processes on inclusions and mechanical properties of cast Al−2Li−2Cu−0.2Zr alloy [J]. Transactions of Nonferrous Metals Society of China, 2019, 29(7): 1375−1382.

[21] DAMANI R J, RUBEŠA D, DANZER R. Fracture toughness, strength and thermal shock behaviour of bulk plasma sprayed alumina−Effects of heat treatment [J]. Journal of the European Ceramic Society, 2000, 20(10): 1439−1452.

[22] OSTAPENKO G, KVASNYTSYA V, TIMOSHKOVA L, SEMENENKO N, DOROGOVIN B. Synthetic andalusite crystals: Morphology and growth features [J]. Journal of Crystal Growth, 1998, 186: 420−426.

[23] THOMPSON G, SKELDON P, SHIMIZU K, WOOD G. The compositions of barrier-type anodic films formed on aluminium in molybdate and tungstate electrolytes [J]. Royal Society of London Philosophical Transactions Series A, 1995, 350: 143−168.

[24] HUSSEIN R O, NIE X, NORTHWOOD D O, YEROKHIN A, MATTHEWS A. Spectroscopic study of electrolytic

plasma and discharging behaviour during the plasma electrolytic oxidation (PEO) process [J]. Journal of Physics D: Applied Physics, 2010, 43(10): 105203.
[25] HUSSEIN R O, NIE X, NORTHWOOD D O. An investigation of ceramic coating growth mechanisms in plasma electrolytic oxidation (PEO) processing [J]. Electrochimica Acta, 2013, 112: 111−119.
[26] SHIMIZU K, THOMPSON G E, WOOD G C. The generation of flaws in anodic barrier-type films on aluminium [J]. Electrochimica Acta, 1982, 27(2): 245−250.
[27] MA Yan-long, ZHOU Xun-xiu, THOMPSON G E, CURIONI M, SKELDON P, ZHANG X, SUN Z, LUO C, TANG Z W, LU F. Anodic film growth on Al–Li–Cu alloy AA2099−T8 [J]. Electrochimica Acta, 2012, 80: 148−159.
[28] CHENG Ying-liang, XUE Zhi-gang, WANG Qun, WU Xiang-quan, MATYKINA E, SKELDON P, THOMPSON G E. New findings on properties of plasma electrolytic oxidation coatings from study of an Al−Cu−Li alloy [J]. Electrochimica Acta, 2013, 107: 358−378.
[29] ORAZEM M E, TRIBOLLET B. An integrated approach to electrochemical impedance spectroscopy [J]. Electrochimica Acta, 2008, 53(25): 7360−7366.
[30] WEN Lei, WANG Ya-ming, ZHOU Yu, OUYANG Jia-hu, GUO Li-xin, JIA De-chang. Corrosion evaluation of microarc oxidation coatings formed on 2024 aluminium alloy [J]. Corrosion Science, 2010, 52(8): 2687−2696.
[31] JORCIN J B, ORAZEM M, PÉBÈRE N, TRIBOLLET B. CPE analysis by local electrochemical impedance spectroscopy [J]. Electrochimica Acta, 2006, 51(8−9): 1473−1479.

NaOH 浓度对铸造铝锂合金微弧氧化膜层显微组织和耐蚀性能的影响

秦 莹[1]，吴国华[1]，Andrej ATRENS[2]，张小龙[1]，张 亮[1]，丁文江[1]

1. 上海交通大学 材料科学与工程学院，轻合金精密成形国家工程研究中心，金属基复合材料国家重点实验室，上海 200240；
2. School of Mechanical and Mining Engineering, the University of Queensland, Brisbane Qld, 4072, Australia

摘 要：采用含有 Na_2WO_4 和不同 NaOH 浓度的硅酸盐系列电解液，利用微弧氧化(MAO)技术在 Al−Cu−Li 合金表面制备陶瓷涂层，研究 NaOH 浓度在 1−9 g/L 范围内对涂层显微组织和腐蚀行为的影响。利用 X 射线衍射(XRD)、X 射线光电子能谱(XPS)和扫描电子显微镜(SEM)对膜层的组成和微观结构进行表征。结果表明，NaOH 促进 MAO 反应中氧化物的生成，使膜层厚度增加。电化学腐蚀测试(极化曲线、交流阻抗谱)和质量损失试验确定膜层的耐蚀性随 NaOH 加入量的增加而提高，且在 7 g/L NaOH 溶液中制备的膜层耐蚀性最优。全浸泡腐蚀试验也给出一致的结果。

关键词：Al−Cu−Li；NaOH；微弧氧化；腐蚀行为

(Edited by Bing YANG)